



Mineral dust emission from the Bodélé Depression, northern Chad, during BoDEX 2005

Martin C. Todd,¹ Richard Washington,² José Vanderlei Martins,^{3,4} Oleg Dubovik,⁴ Gil Lizcano,¹ Samuel M'Bainayel,⁵ and Sebastian Engelstaedter²

Received 6 February 2006; revised 4 May 2006; accepted 10 August 2006; published 22 March 2007.

[1] Mineral dust in the atmosphere is an important component of the climate system but is poorly quantified. The Bodélé Depression of northern Chad stands out as the world's greatest source region of mineral dust into the atmosphere. Frequent dust plumes are a distinguishing feature of the region's climate. There is a need for more detailed information on processes of dust emission/transport and dust optical properties to inform model simulations of this source. During the Bodélé Dust Experiment (BoDEX) in 2005, instrumentation was deployed to measure dust properties and boundary layer meteorology. Observations indicate that dust emission events are triggered when near-surface wind speeds exceed 10 ms^{-1} , associated with synoptic-scale variability in the large-scale atmospheric circulation. Dust emission pulses in phase with the diurnal cycle of near-surface winds. Analysis of dust samples shows that the dust consists predominantly of fragments of diatomite sediment. The particle size distribution of this diatomite dust estimated from sun photometer data, using a modified Aeronet retrieval algorithm, indicates a dominant coarse mode (radius centered on $1\text{--}2 \mu\text{m}$) similar to other Saharan dust observations. Single-scattering albedo values are high, broadly in line with other Saharan dust even though the diatomite composition of dust from the Bodélé is likely to be unusual. The radiative impact of high dust loadings results in a reduction in surface daytime maximum temperature of around 7°C in the Bodélé region. Using optical and physical properties of dust obtained in the field, we estimate the total dust flux emitted from the Bodélé to be $1.18 \pm 0.45 \text{ Tg per day}$ during a substantial dust event. We speculate that the Bodélé Depression ($\sim 10,800 \text{ km}^2$) may be responsible for between 6–18% of global dust emissions, although the uncertainty in both the Bodélé and global estimates remains high.

Citation: Todd, M. C., R. Washington, J. V. Martins, O. Dubovik, G. Lizcano, S. M'Bainayel, and S. Engelstaedter (2007), Mineral dust emission from the Bodélé Depression, northern Chad, during BoDEX 2005, *J. Geophys. Res.*, *112*, D06207, doi:10.1029/2006JD007170.

1. Introduction

[2] Atmospheric aerosols influence the Earth's radiation budget and are thus an important component of the Earth's climate system, and likely play an important role in global climate change. Indeed, aerosols are one of the greatest sources of uncertainty in interpretation and projection of past and future climate change [Ramaswamy *et al.*, 2001]. Aerosols are produced from a range of sources including

volcanic eruptions, anthropogenic pollution, biomass burning, the oceans and wind-blown terrestrial mineral dust. The distribution, properties of mineral dust and its climate impact are poorly understood, despite evidence that the radiative impact may be comparable to that of anthropogenic sulphate aerosols [Ramaswamy *et al.*, 2001]. In many regions, mineral dust is the biggest contribution to atmospheric optical thickness [Tegen *et al.*, 1997], and evidence exists of increasing dust production in recent decades [Goudie and Middleton, 1992; Prospero and Lamb, 2003]. Dust also plays an important role in terrestrial and oceanic biogeochemical cycles and it has been suggested that Saharan dust plays a key role in fertilisation of soil systems in the Sahel and the Amazon basin [Swap *et al.*, 1992].

[3] The direct and indirect radiative forcing effects of mineral dust aerosols have been studied from simulations [e.g., Miller and Tegen, 1998; Collins *et al.*, 2001; Ginoux *et al.*, 2001; Weaver *et al.*, 2002; Myhre *et al.*, 2003] and observations [e.g., Hsu *et al.*, 2000; Kaufman *et al.*, 2001;

¹Department of Geography, University College London, London, UK.

²Climate Research Laboratory, Oxford University Centre for the Environment, University of Oxford, Oxford, UK.

³University of Maryland Baltimore County, Baltimore, Maryland, USA.

⁴Also at NASA Goddard Space Flight Center, Greenbelt, Maryland, USA.

⁵Direction des Ressources en Eau et de la Météorologie (DREM), N'Djamena, Chad.

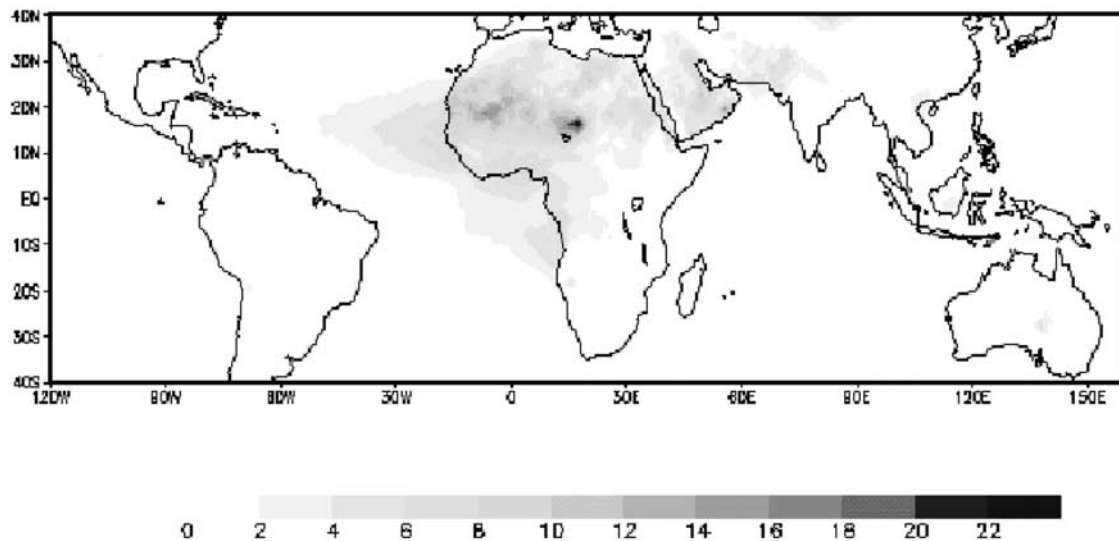


Figure 1. Annual mean aerosol index from TOMS (1980–1993, arbitrary units $\times 10$).

Haywood *et al.*, 2003a, 2003b; Highwood *et al.*, 2003; Tanré *et al.*, 2003]. These studies indicate that the radiative impact of dust is complex. Dust backscatters solar radiation to space and acts like a greenhouse gas to absorb upwelling terrestrial radiation. The net radiative effect of dust is influenced by underlying surface properties and dust optical properties. Over oceans the radiative forcing in the solar spectrum can be as high as -130 Wm^2 locally [Haywood *et al.*, 2003b] whilst over the land the net effect may be generally positive [Weaver *et al.*, 2002]. Haywood *et al.* [2005] estimate the longwave radiative effect to be up to $+50 \text{ Wm}^2$ in cloud free regions of the Sahara. As a result, the magnitude and even the sign of dust radiative forcing remains uncertain [Ramaswamy *et al.*, 2001]. Individual Saharan dust events have been estimated to induce a global mean net radiative forcing of -0.4 Wm^2 [Myhre *et al.*, 2003]. There is clearly a need for detailed information on dust physical and optical properties to test the assumptions made in calculations of radiative forcing and the models used for simulation of dust emission and transport [Kinne *et al.*, 2003], as well as for retrieval of aerosol properties from satellite information. These radiative transfer models require a range of information including aerosol optical thickness (AOT), phase function, single-scattering albedo (ω_0 , the ratio of scattering to scattering plus absorption), itself largely dependent on the complex part of the refractive index, and particle size distribution.

[4] Satellite sensors providing near-global representation of aerosols, namely the Total Ozone Mapping Spectrometer (TOMS) and the Multi-angle Imaging Spectro-Radiometer (MISR), show that most of the world's mineral dust is associated with a small number of key preferential source regions [Herman *et al.*, 1997; Torres *et al.*, 2002; Washington *et al.*, 2003; Zhang and Christopher, 2003]. Within the Sahara the TOMS aerosol index (Figure 1), TOMS AOT (not shown), and the MISR AOT products (not shown) all highlight the Bodélé Depression in northern Chad as the region with consistently the highest mineral dust aerosol loadings. This region is therefore the dustiest place on Earth [Washington *et al.*, 2003] and, unlike other

regions of the Sahara, is a major dust source throughout the year. The Bodélé Depression is the deepest part of the paleolake basin Mega-Chad, which was exposed when the lake dried up some 5000 years BP.

[5] That the Bodélé Depression is such a dominant dust source is due to the collocation of (1) an extensive source of readily erodible diatomite sediment ($\sim 10,800 \text{ km}^2$) centered near 17°N , 18°E (Figure 2a) which is the source of the major dust plumes characteristic of the region (Figure 2c) and (2) locally strong winds associated with the Bodélé Low-Level Jet (LLJ, Figure 3a) [Washington and Todd, 2005; Washington *et al.*, 2006]. The Bodélé LLJ results from the acceleration of the mean northeasterly “Harmattan” wind flow of North Africa due to the presence of the Tibesti and Ennedi massifs which rise around 2600 m to the north, and 1000 m to the east, respectively, above the Bodélé Depression (Figure 3a). It is likely that combination of a gap wind and downslope wind forcing creates the LLJ [Washington and Todd, 2005; Washington *et al.*, 2006]. The LLJ and diatomite sediment interact to produce extensive dust plumes (Figure 2c), which extend as singular features up to 1000 km downwind and occur around 100 times per year [Koren and Kaufman, 2004; Washington *et al.*, 2006]. The dust plumes of the Bodélé Depression are a most remarkable geophysical phenomenon.

[6] The Bodélé Depression is an extremely remote region about which little is known in the scientific literature. To address this, the Bodélé Dust Experiment (BoDEx), an international, multidisciplinary field project was undertaken in February–March 2005 to obtain fundamental information on processes of dust emission and transport and the properties of dust from the Bodélé region (<http://www.geog.ox.ac.uk/research/projects/bodex/>). By obtaining observations directly within the world's primary source region BoDEx 2005 is rather different from most previous studies of Saharan dust in which observations are made at locations remote from the source regions. Kinne *et al.* [2003] report that many dust models underestimate dust emission from key source regions. The rationale for this work is therefore as follows: (1) The Bodélé Depression is the world's greatest

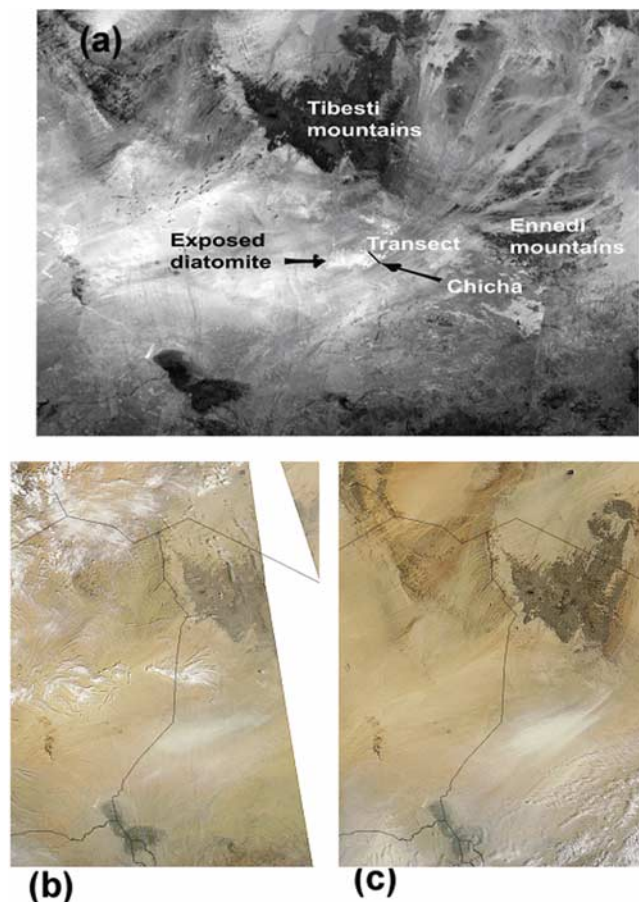


Figure 2. (a) MODIS channel 4 surface reflectance (8 day composite 27/2/05–6/3/05); (b) MODIS true color composite (channels 3, 4, and 1) image for 1245 UTC 4 March 2005; (c) as in Figure 2b, but for 09:50 11 March 2005. The location of the BoDEX 2005 field site at Chicha (16.9°N, 18.5°E) is indicated in Figure 2a. The line in Figure 2a indicates the transect used in dust flux calculation (section 6).

dust source because of its highly unusual geomorphological and climatological characteristics, (2) a key requirement of dust models which estimate global dust emission and associated climate impact is to simulate accurately dust emission/transport from this key source region, and (3) detailed information of key processes in the Bodélé during dust events is therefore required for model parameterisation, calibration and validation. Accordingly, in this paper we address the following: (1) What is the relationship between the dust emission events and the local wind conditions? (section 3). (2) What are the values of the critical physical and optical properties of the dust that determine the radiative effect, and are these similar to other Saharan dust sources? (section 4) (3) What is the effect of dust on the local climate? (section 5). (4) What is the magnitude of mass flux of dust from the Bodélé Depression? (section 6).

2. Data and Methods

[7] The BoDEX field campaign ran from 28 February to 13 March 2005. The instrumentation used to monitor

aerosol properties consists of a suite of ground based instruments: (1) a Cimel C-318 sun-sky spectral radiometer calibrated and upgraded as part of the NASA Aerosol Robotic Network (AERONET) protocol [Holben *et al.*, 1998] and (2) a Microtops handheld sun photometer instrument, manufactured by Solar Light Co. In addition, Meteorological observations of wind speed, air temperature and solar radiation (over the wavelength range 300–1000 nm)

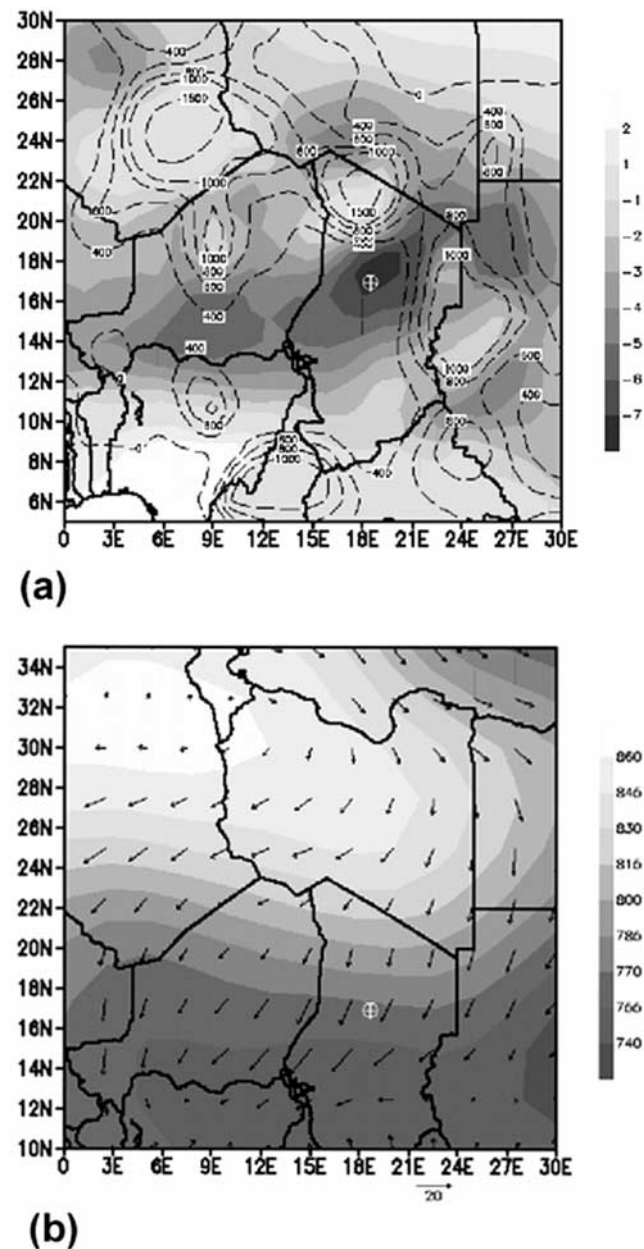


Figure 3. Characteristics of the wind regime in the study region. (a) Long-term mean 925 hPa zonal wind speed (shaded, ms^{-1}) during March (1979–2001) from ERA-40 reanalysis data. Westerly (easterly) winds have positive (negative) values. Contours indicate surface topography (m). (b) Geopotential height at 925 hPa (gpm, shaded) and 925 hPa wind speed and direction (ms^{-1} , arrows) for 06z, 10 March 2005 from NCEP reanalysis data. Cross in circle marks location of BoDEX field site in both figures.

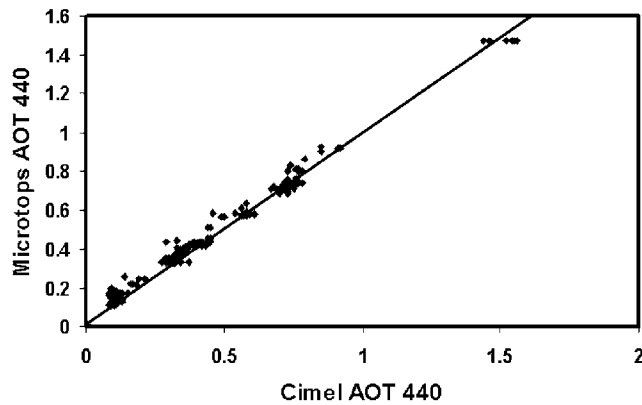


Figure 4. Comparison of near-coincident observations of AOT_{440} from the Cimel and Microtops instruments.

were made at 2 min intervals using a Davis Vantage Pro weather station mounted at 2 m. The instruments were located at 16.88°N, 18.53°E, and elevation 179 m (Figure 2a). The location was selected for logistical and scientific reasons. The site is relatively accessible and has a supply of groundwater. The field site is located at the southeastern edge of the exposed diatomite deposits, which is the primary dust plume source region (Figure 2), enabling direct observations of both surface dust emission processes and the atmospheric characteristics.

[8] The Cimel 318A spectral radiometer is a solar powered robotically pointed sun and sky spectral radiometer. This instrument made sun and sky observations at four wavelengths; 440, 670, 870 and 1020 nm with further observation in the water vapour absorption channel of 940 nm. The Cimel makes two basic measurements, direct sun and sky, within programmed sequences. AOT is calculated from spectral extinction of direct beam radiation at each wavelength on the basis of the Beer-Bouguer Law. Attenuation due to Rayleigh scatter, absorption by ozone (from interpolated ozone climatology atlas), and gaseous pollutants are estimated and removed to isolate the AOT. A sequence of three such measurements is taken 30 sec apart creating a triplet observation per wavelength for cloud screening purposes.

[9] The Cimel measures the sky radiance in four spectral bands along the solar principal plane (i.e., at constant azimuth angle, with varied scattering angles) up to nine times a day and along the solar almucantar (i.e., at constant elevation angle, with varied azimuth angles) up to six times a day. The approach is to acquire aureole and sky radiances observations through a large range of scattering angles from the sun through a constant aerosol profile to retrieve size distribution, phase function and AOT. Sky radiance measurements are inverted using a new refinement of the *Dubovik and King* [2000] scheme to provide aerosol optical properties, size distribution and phase function over the particle size range of 0.05 to 15 μm radii. In this new scheme, aerosols are assumed to be randomly oriented spheroids as in *Dubovik et al.* [2002b] but in addition (1) the spheroid mix is refined and extra constraints were used for limiting the concentrations of fine particles with radii 0.05 μm [*Dubovik et al.*, 2006] and (2) surface albedo were assumed on the basis of surface reflectance

climatologies derived from satellite observations by *Moody et al.* [2005]. These refinements to *Dubovik and King* [2000] aerosol retrieval are to be included in an operational new version processing of AERONET data that is currently under development.

[10] There are notable gaps in the record provided by the Cimel during BoDEx 2005 because of (1) the instrument sensor head overheating during the local afternoon resulting in corrupted data and so, generally, observations are limited to the morning and (2) During the periods of intense dust emission the Cimel could not operate because of the potential for damage to the instrument motor and optics from saltating sand particles. The Bodélé region is generally cloud free during the boreal spring season. Nevertheless cirrus clouds associated with the subtropical jet stream do occur in the region and were present in the study period. The Cimel data were screened for the presence of clouds using the standard AERONET method described by *Smirnov et al.* [2000]. These cloud screened data are referred to as Aeronet level 1.5 data. The cloud screening algorithm uses a number of decision rules based on the variability of AOT values at short timescales (i.e., within the triplet observations and within a day). Cloud identification is based on the assumption that temporal variability in AOT due to clouds is likely to be higher than that associated with aerosols. This assumption may be violated when (1) temporal variability in cloud characteristics is low and (2) when temporal variability of aerosols is high. Such a condition may apply to the BoDEx data since (1) the only clouds observed are thin cirrus clouds with low temporal variability and (2) the site is a dust source region where dust production is highly variable because of microscale and mesoscale variability in surface wind speed.

[11] The Microtops instrument provides observations of AOT every 30 min each day from 0500 UTC to 1600 UTC. The only break in the record occurred during the periods of most intense dust production when the sun was not visible. As such, the Microtops instruments provide a useful additional source of information on AOT. The Microtops instrument has filters at 440, 675, 870, 936 and 1020 nm. Microtops observations coincident with the Cimel observations were screened for clouds using the Cimel record. Microtops observations during periods when the Cimel was inoperable were cloud screened using a combination of manual surface based observations and satellite observations of cirrus occurrence. Near-coincident observations of AOT from the Microtops and the Cimel are in close agreement (Figure 4) providing confidence in the stability of the instruments and in the ability of the Microtops to substitute for periods of Cimel inactivity.

[12] A sample of airborne dust was collected on a sticky scanning electron microscope (SEM) stub at the field site on 10 March 2005. The stub was positioned at 2 m height to capture dust transported largely by suspension. The samples were placed on a 3 mm pin type stub with a carbon tab. Energy dispersive analysis was done on an EDAX system equipped with a Super Ultra Thin Window (SUTW). The samples were examined in a Phillips XL30 Environmental scanning electron microscope.

[13] A range of large-scale atmospheric information was analysed in support of the field data. Information on large-scale atmospheric conditions was obtained from ERA-40

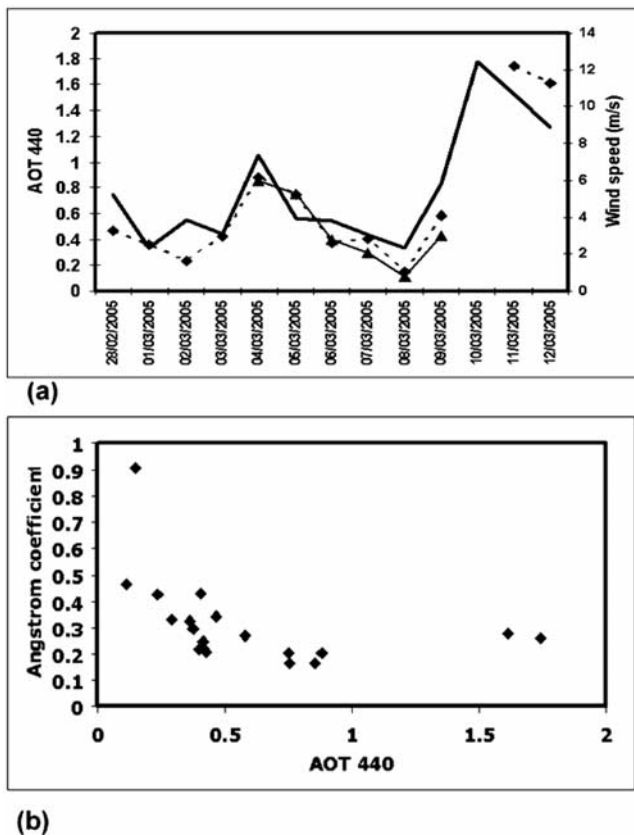


Figure 5. Daily average values observed during BoDEx 2005 of (a) AOT₄₄₀ from the Cimel 318 (solid thin line with triangle markers) and Microtops instrument (dotted line with diamond markers) and daily mean 2 m wind speed (solid thick line), (b) AOT₄₄₀ and Angstrom parameter from Microtops and Cimel instruments.

and NCEP reanalysis data sets and composite MODIS satellite imagery. Parcel trajectories were calculated using the British Atmospheric Data Centre (BADC) trajectory service, using atmospheric winds from the ECMWF operational analysis fields at 1.125° resolution. An atmospheric simulation was made using the Pennsylvania State University/National Center for Atmospheric Research numerical model MM5 over the Bodélé domain. MM5 is a nonhydrostatic, primitive equation model using terrain following coordinates [Dudhia, 1993; Grell *et al.*, 1994]. It was configured with two nested domain grids in a two-way nesting. The mother domain has 81 km resolution and covers the region 4.4–34.2°N, 4.0–36.0°E, whilst the nest domain has a resolution of 27 km over 9–24°N, 9–24°E, roughly centered on the Bodélé. Lateral boundary conditions were provided by 6 hourly NCEP Reanalysis fields. The Noah Land Surface Model was employed in the simulation using MRF planetary boundary layer scheme. The simulation ran for the period 25 February to 15 March 2005.

3. Dust and Wind Conditions During BoDEx 2005

[14] During the 14 day period of BoDEx 2005 the region experienced a wide range of dust conditions. There were

substantial dust emission events on 10, 11, and 12 March. On these days dust emission was severe with surface visibility restricted at times to approximately 20 m and dust plumes were clearly visible from MODIS imagery (Figure 2c). Moderate dust emission over shorter periods of a few hours occurred on 3 further days (28 February, 4 and 9 March), when small plumes were visible from MODIS imagery (Figure 2b). On the remaining days dust emission from the field region was negligible (Figure 2a).

[15] The time series of AOT (Figure 5a) illustrates this variability in dust emission. AOT₄₄₀ values are ~0.15 on the clearest days (e.g., 8 March). Elevated AOT₄₄₀ values are apparent during the moderate dust events of 28 February, 4 March (AOT₄₄₀ = 0.86), and 9 March. The major dust events of 10–12 March (observed using the Microtops sensor only) are associated with daily mean AOT₄₄₀ values of up to 1.62 on 11 March. On 10 March one single instantaneous AOT₄₄₀ value of 6.4 was observed. An instantaneous peak AOT₄₄₀ value of 3.6 was recorded on 11 March. It must be noted however that the error in these observations, when the sun is partially obscured by dust, is high. These Microtops observations obtained during 10–12 March are actually indicative of periods of relatively low dust emission during the afternoon only when the sun was just visible. During the mornings of 10–12 March no observations were possible and aerosol loadings are therefore higher than those indicated by the afternoon Microtops results.

[16] The variability in daily mean AOT corresponds closely to the variability in daily mean surface wind speed (Figure 5a). This is consistent with the condition that the aerosols are produced locally from the zone of exposed diatomite sediments (except on 5 March: see below). Variability in daily mean near-surface wind speed is modulated by variability in the large-scale circulation. Specifically, the flow direction and velocity of the Bodélé LLJ is controlled substantially by the intensity and position of the Libyan high-pressure system. The major dust events during BoDEx 2005 are clearly associated with increased intensity in the LLJ caused by eastward ridging of the Libyan High (Figure 3).

[17] Despite the primary role that the large-scale synoptic conditions play in producing the large dust events, the local diurnal cycle remains important. On all days a pronounced diurnal cycle in surface wind speeds is observed with maxima (minima) close to 0900 UTC (2000 UTC) (local time is UTC + 1 hour). That strongest winds at the surface typically occur in the mid morning is due to mixing of momentum from the LLJ down to the surface by radiative heating. This is also evident during the large dust event of 10–12 March when 15 min average maximum (minimum) values of ~14 ms⁻¹ (~2–8 ms⁻¹) were recorded near 0800 [2000] UTC (Figure 6a). On these days dust emission reflected this diurnal cycle, occurring in pulses of ~18 hours duration on the 10 and 11 and ~13 hours on 12 March. Although no photometer observations were possible during the mornings because of excessively high dust loadings, after 1200 UTC on 11 and 12 March AOT observations from the Microtops were possible as the atmosphere cleared, and a coincident decline in AOT₄₄₀ and wind speed was recorded (Figure 6a). From this we can infer that dust transport out of the region within the LLJ

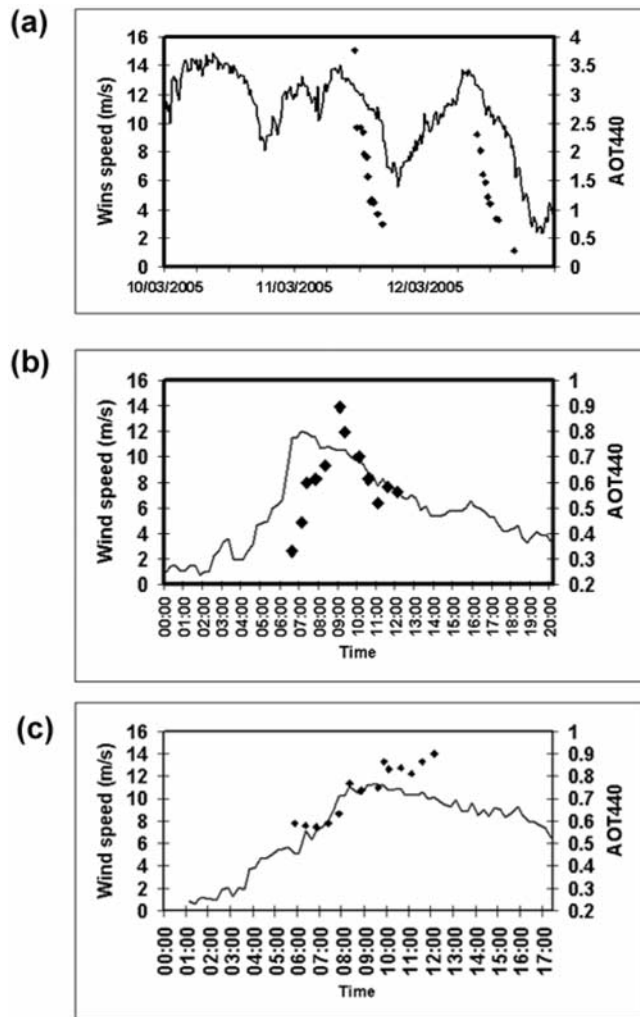


Figure 6. Instantaneous AOT_{440} (diamonds) and 15 min mean 2 m wind speed (line, ms^{-1}) during (a) 10–12 March 2005 (b) 9 March 2005 (c) 4 March 2005. All times are UTC.

exceeded the rate of surface emission after 1200 UTC on both days resulting in falling AOT values. During the smaller dust events of 9 and 4 March the AOT_{440} cycle lags wind speed by about 1 hour (Figures 6b and 6c). On 4 March, AOT_{440} values remained elevated throughout the afternoon (not shown) because of advection of dust into the Bodélé from the remote Ennedi region to the east, visible on the MODIS imagery (Figure 2b). Wind direction was ENE on 4 March compared to NNE or NE on all other dust days. This advection of dust from remote sources persisted during 5 March when AOT values remained relatively high but wind speeds were too low for local dust emission (Figure 5a).

[18] One of the largest uncertainties in modeling dust is the dust emission from source regions such as the Bodélé. In most models the processes of dust uplifting are parameterized as a function of wind speed, soil water content, surface roughness and particle size and density [e.g., *Ginoux et al.*, 2001; *Zender et al.*, 2003; *Tegen et al.*, 2002]. The threshold wind speed for dust emission is a critical factor in dust

models. From consideration of coincident observation of wind speed, AOT, and visual observations of visibility, saltation and surface dust flux we estimate the threshold wind velocity (at 2 m over 15 min) for dust emission to be 10.0 ms^{-1} . This is consistent with the duration of dust emission on 28 February, 4 and 9–12 March and the absence of substantial emission on other days when wind speeds never exceeded 10.0 ms^{-1} . This estimate is also very close to the minimum estimated dust plume advection rate for the Bodélé derived from satellite data by *Koren and Kaufman* [2004]. This threshold wind speed is considerably greater than those observed elsewhere. *Gillette* [1977] suggests a threshold wind speed of $6\text{--}7 \text{ ms}^{-1}$ whilst *Park and In* [2003] define values of $6.0\text{--}9.5 \text{ ms}^{-1}$ (at 10 m height) for various surface types in China from statistical comparison of wind speed and dust storm occurrence. On the basis of various studies, *Tegen and Fung* [1994] use a threshold of 6.5 ms^{-1} (at 10m) in their global dust model. This disparity may reflect the rather unusual process by which fine dust is liberated in the Bodélé through self-abrasion of mobilised diatomite flakes [*Giles*, 2005].

4. Physical and Optical Properties of Bodélé Dust

[19] SEM analysis of the dust particles on the stub indicates that the dust is dominated by fragmented fossil diatoms from the dry lake bed of the Bodélé (Figure 7). The dominant species are the planktonic centric diatom *Aulacoseira* and *Stephanodiscus*. In addition, large quartz particles are evident, which have their origin in the desert surrounding the depression. The quartz grains are $50\text{--}250 \mu\text{m}$ in size such that they represent the saltating particles not involved in long-range transport. The barchan dunes which hold substantial quantities of quartz are largely restricted to the eastern side of the Bodélé Depression surrounding the BoDEx field site. The majority of the central and western Bodélé is relatively free of sources of quartz. Trace quantities of evaporite products such as halite are apparent. From this we can infer that the dust emitted from the Bodélé is predominantly composed of fragmented fossil diatoms.

[20] Retrievals of aerosol size distribution from Cimel data using the revised Aeronet retrieval show a dominant coarse mode centered on $1.5\text{--}2.0 \mu\text{m}$ and a minor fine mode centered close to $0.5 \mu\text{m}$ (Figure 8a). The coarse mode becomes more dominant during the dust events (4 and 9 March). There is an order of magnitude increase in the volume concentration of the coarse mode during the moderate dust events compared to “clear” conditions. The coarse mode is characteristic of dust properties observed elsewhere in the Sahara and other desert regions, e.g., the long-term observations of *Dubovik et al.* [2002a] and short-term observations of *Highwood et al.* [2003]. However, the minor but noticeable presence of fine particles with radii $<1 \mu\text{m}$ is rather unusual for desert dust. Estimates of the particle size distribution based on electron microscopy of in situ samples of dust collected on nucleopore filters using a vacuum pump dust sampler during BoDEx 2005 are very similar (*J. V. Martins et al.*, manuscript in preparation, 2006). Retrievals using the current operational Aeronet scheme with an assumption of spheroidal particles (not shown) indicate a pronounced ultra fine mode centered close to $0.05 \mu\text{m}$, which is not shown in SEM analysis of

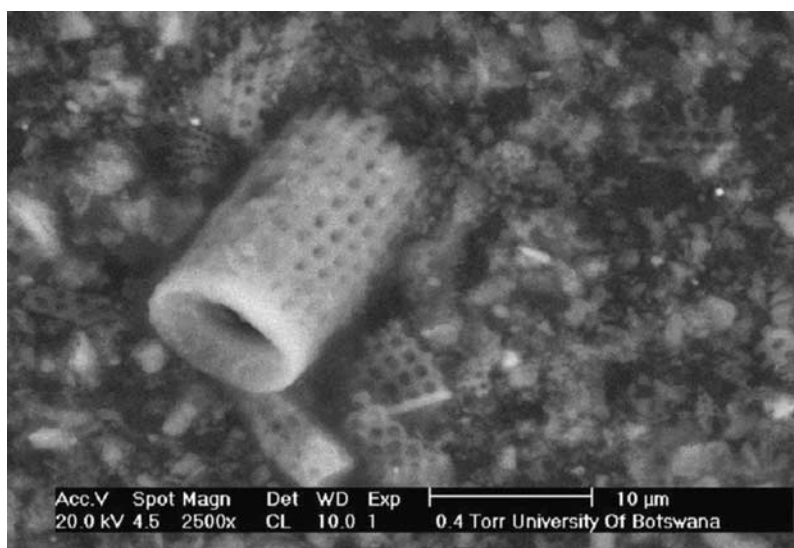


Figure 7. SEM image of dust sample collected on 10 March 2005 at the BoDEx field site. Clearly visible are crushed diatom fragments from the dry paleolake bed.

in situ dust samples (although the technique is capable of resolving this mode if it existed) (J. V. Martins et al., manuscript in preparation, 2006) nor the new retrieval, and is likely to represent an artefact of the retrieval. This demonstrates the value of the new retrieval scheme.

[21] The shape of the particle size distribution is similar in relatively clear and dusty conditions consistent with the condition that the study site is a source region such that the atmosphere is dominated by locally produced aerosols. The median size of the coarse mode is $1.9 \mu\text{m}$, and the effective radius is $1.66 \mu\text{m}$ (for cases when dust is locally produced). These are close to those figures derived from sun-sky radiometer data elsewhere for desert dust and from other in situ observational methods [e.g., Dubovik et al., 2002a, and references therein]. The spectral dependence of AOT can also be utilised to obtain information on the size of dust particles. The Ångström parameter, which is indicative of the average spectral behaviour of AOT, was derived from both Cimel data and Microtops data on the basis of daily mean AOT. The results show a broadly inverse relationship with AOT (Figure 5b) for daily mean values, suggestive of a shift toward coarse particles during dust outbreak events of 4, 9, and 11–12 March. During the major dust event on 10 March only one observation was obtained (not shown in Figure 5) and indicates an extremely low Ångström value of 0.08. The daily mean Ångström values are in line with those reported previously in the Sahara and elsewhere [e.g., Smirnov et al., 2000; Pinker et al., 2001; Dubovik et al., 2002a].

[22] Observations from the Aeronet Cimel instrument at Ilorin, southwest Nigeria ($8^\circ, 19'N, 4^\circ, 20'E$), are also instructive. There is strong evidence of dust transport to this region from the Bodélé. Parcel trajectories from the Bodélé over 10–12 March are toward the southwest reaching southwest Nigeria after approximately 3 days (not shown). This pattern of long-range dust transport to the southwest from the Bodélé during BoDEx 2005 is very typical of conditions during the winter/spring period [Washington et al., 2006]. Dust emitted from the Bodélé

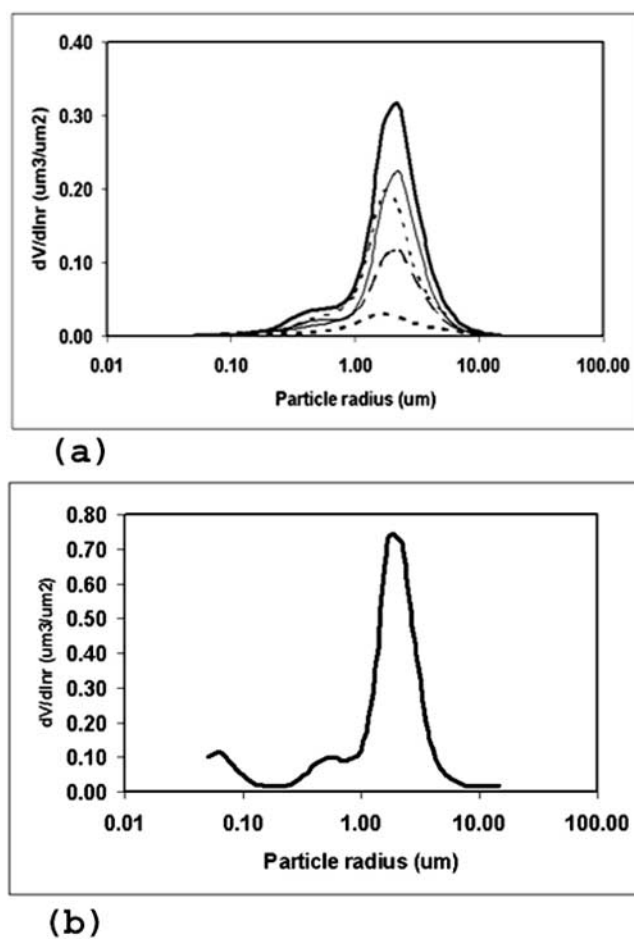


Figure 8. Particle size distribution for (a) daily mean at Bodélé using the “new” Aeronet retrieval (4 March: solid thick line, 6 March: thin dotted line, 7 March: dashed line, 8 March: thick dotted, line 9 March: solid thin line). (b) Mean for 13–15 March observed at Ilorin, Nigeria, using standard Aeronet retrieval with spheroidal particle assumption.

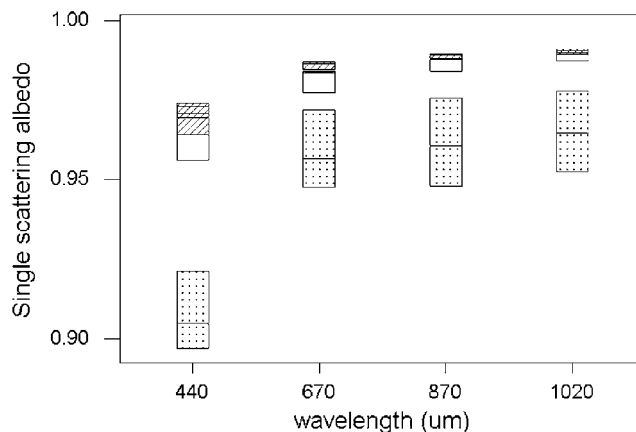
Table 1. Summary of Dust Optical Properties Observed During BoDEx 2005 Using Revised Aeronet Retrieval on Cimel Data

Parameter	Value
Aerosol optical thickness at 440 nm (mean/min/max)	0.41/0.08/1.56
Ångstrom parameter (mean/min/max)	0.24/0.06/0.45
Mean single scattering albedo (ω_o) (440,670,870,1020 nm) ^a	0.969/0.986/0.989/0.990
Real part of refractive index (440,670,870,1020 nm) ^a	1.46/1.47/1.45/1.44
Imaginary part of refractive index (440,670,870,1020 nm) ^a	0.002/0.001/0.001/0.001
Mean (standard deviation) volume concentration ($\mu\text{m}^3/\mu\text{m}^2$) ^a	0.27 (0.05)
Effective particle radius (and standard deviation) of all/fine mode/coarse mode (μm) ^a	1.1 (0.12)/0.20 (0.02)/1.66 (0.12)

^aDays where mean AOT₄₄₀ > 0.3 and when dust is locally produced.

on 10–12 March was detectable from observations at the Aeronet station at Ilorin, Nigeria, approximately 3 days later, with enhanced AOT₄₄₀ values (in excess of 1.2) compared to the 3 days immediately prior (~ 0.5 – 0.8). We are confident that the AOT at Ilorin was dominated by mineral dust rather than biomass burning aerosols because of the very low Ångstrom coefficients observed on these days (~ 0.2). Retrievals of particle size distribution with the standard Aeronet retrieval from data obtained at Ilorin on 13–15 March (using an assumption of spheroidal particles, Figure 8b), 3 days after the large Bodélé dust event of 10–12 March, show that the dominant coarse mode (and noticeable fine mode) is very similar to that observed at the Bodélé source. The magnitude of the coarse mode dust volume at Ilorin during 13–15 March is approximately three times that from the Bodélé estimates of the “moderate” dust event of 4–5 March. On the basis of analysis of the Bodélé data using the “new” Aeronet retrieval we can assume that the ultrafine particle mode ($<0.1\mu\text{m}$) in the Ilorin data is artificial.

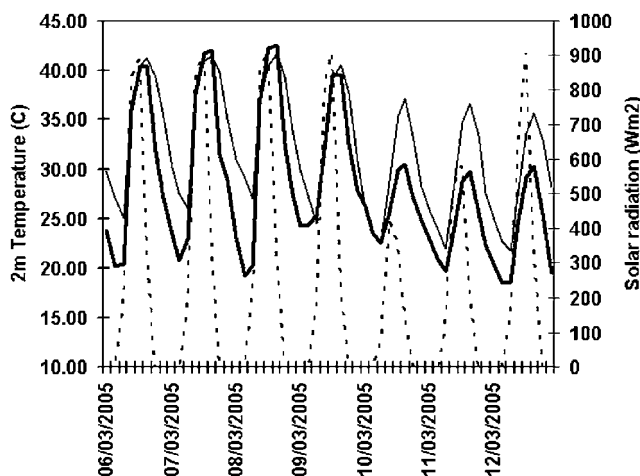
[23] The optical characteristics of Bodélé dust retrieved from the Cimel instrument are summarized in Table 1. Mean ω_o values (for the days when AOT₄₄₀ exceeded 0.3 and when we are confident that the dust sources is local) range from 0.969 at 441 nm to 0.99 at 1022 nm (Figure 9). Similar values are obtained from the Aeronet instrument at Ilorin, Nigeria, downwind from the Bodélé over the period 13–15 March (Figure 9). On 5 March when the dust source was the Ennedi region to the east of the Bodélé ω_o values are significantly lower (Figure 9). That ω_o values are high for local sources of Bodélé dust and lower for remote dust is broadly corroborated by the analysis of in situ dust samples from the Bodélé (J. V. Martins et al., manuscript in preparation, 2006) The result adds weight to the perspective that absorption of solar radiation by dust at wavelengths greater than 550 nm is very weak but that absorption in the blue spectral range can be pronounced for certain dust source regions [e.g., Kaufman et al., 2001; Dubovik et al., 2002a, and references therein]. This result has important implications for the magnitude of associated dust radiative forcing. How-

**Figure 9.** Box plot of wavelength dependence of single-scattering albedo of dust. Plot shows mean and 95% confidence intervals for observations at Bodélé on 4 and 9 March 2005 (hatched box), 5 March (dotted box) and from Ilorin, Nigeria, on 13–15 March (clear box). Horizontal line in each box shows the mean value.

ever, because of the short record in this study, this conclusion must be treated with caution.

5. Impact of Dust on Surface Heating

[24] High-aerosol loadings during the major dust event of 10–12 March had a substantial impact on surface shortwave radiation and as a result on air temperatures. Solar radiation flux at the surface was substantially reduced (Figure 10). The daily maximum solar flux observed on 10, 11, and 12 March was only 45%, 60%, and 80%, respectively, of the pre-event values on 8 March. Note that on 12 March dust emission occurred only during the local morning such that solar radiation values were suppressed only prior to 1200 UTC. Daily maximum temperatures fell from 43.0°C on 8 March to only 30.9°C, 30.6°C and 30.7°C on 10–12 March

**Figure 10.** Time series from 6–12 March at the BoDEx site of 2 m temperature observed (solid thick line), simulated near-surface temperature surface using MM5 (solid thin line) and observed solar radiation (dotted line). All times are UTC.

(Figure 10) a drop of more than 12°C. Temperature changes result from a combination of horizontal and vertical temperature advection and diabatic heating (consisting of radiant fluxes and surface heat fluxes, which are dominated by sensible heat flux). Given the strength of the northeasterly wind anomalies (Figure 3b) and the reduction in shortwave radiation flux it is likely that both advective and diabatic heating contributions are substantial. We can estimate the magnitude of each of these components by comparing our observed surface meteorological observations with data from the MM5 model simulation. The MM5 model includes the dynamical processes but does not simulate the radiative effect of enhanced atmospheric aerosols such that temperature changes in the model will be dominated by temperature advection. During the dust-free days (6–8 March) the model simulates very accurately the magnitude and variability in daily maximum temperatures. During dust-free conditions nighttime temperature minima are spatially highly variable and consistently overestimated by the model at Chicha although not at Faya (19°10'E, 18°N) located some 120 km northeast of Chicha where the WMO station (WMO code 64753) provides a limited amount of data (not shown). During the dust event of 10–12 March, MM5 overestimates daily maximum temperatures by about 7°C (Figure 10). Therefore of the ~12°C depression in daily maximum temperatures observed over 10–12 March relative to 8 March, only about 5°C can be accounted for by horizontal and vertical temperature advection in the MM5 model (Figure 10). We can infer that the net radiative effect of the high-aerosol loadings (dominated by shortwave fluxes during the day) at the surface is to reduce near-surface maximum temperature by about 7°C.

6. Estimated Dust Mass Flux From the Bodélé Depression During BoDEx 2005

[25] Quantifying the mass flux of dust from the world's major dust source regions is vital to addressing key questions regarding global and regional biogeochemical cycles [e.g., *Swap et al.*, 1992] as well as to evaluate model estimates. Here, we utilise information obtained in the field to estimate the total dust flux from the Bodélé during the 3 day dust event of 10–12 March 2005. The dust flux over a point (F_p , $\text{g m}^2 \text{s}^{-1}$) can be expressed as

$$F_p = M \times U, \quad (1)$$

where M is the column-integrated dust mass (gm^2) and U the vertically integrated wind speed (ms^{-1}) through the dust layer which we assume to be <500 m over the source region. This assumption is based on parcel trajectories over the region and estimates of dust plume height from MISR satellite data which suggest that the dust layer is less than 600 m height as far as 1000 km downwind of the Bodélé [*Koren et al.*, 2006]. We estimate M as a function of atmospheric AOT_{440} . Estimates of AOT_{440} are not available during nighttime nor during the peak dust conditions, so we estimate AOT_{440} at 30 min time steps from near-surface wind speed on the basis of the observed association of AOT_{440} and 30 min average wind speed during the field period. Consistent with the dust emission schemes of many models [e.g., *Ginoux et al.*, 2001; *Zender et al.*, 2003; *Tegen*

et al., 2002] in which dust emission or saltation is proportional to U^3 , we find that the regression coefficient between AOT_{440} and U_{30}^3 is 0.088, ($r^2 = 0.78$, $\text{SE} = 0.005$) where U_{30} is the 30 min average 2 m wind speeds in excess of the emission threshold of 10.0 ms^{-1} .

[26] Estimates of AOT_{440} are then converted to dust volume (V , $\text{m}^3 \text{m}^2$) on the basis of the close linear association between AOT_{440} and dust volume V derived from the Cimel retrievals during our sample. The regression coefficient between V and $(\text{AOT}_{440} - \text{AOT}_{(\text{B})440})$ is 0.62 ($r^2 = 0.96$, $\text{SE} = 0.0146$) where $\text{AOT}_{(\text{B})440}$ is the background AOT of dust-free conditions. Dust volume, V , is then converted to dust mass, M (gm^2), assuming a dust density of 2.1 gcm^3 obtained from laboratory analysis of numerous samples of fine diatomite sediment obtained from locations in the Bodélé. Then, from equation (1), dust flux, F_p , is estimated every 30 min and then integrated over the 3 day period.

[27] This estimate of F_p represents the dust flux passing the BoDEx field site. To determine the mass flux from the entire Bodélé region, we first calculate the flux crossing a transect, perpendicular to the mean wind direction (over the 3 days 10–12 March), extending from the field site at the southern boundary of the area of exposed diatomite sediment to the northern boundary (Figure 2a). The dust flux F is the product of F_p and the length of this cross section (43,000 m) (following the method of *Kaufman et al.*, 2005). For the 3 day period 10–12 March, $F = 0.29 \text{ Tg}$. It is clear from analysis of dust plumes from MODIS data and experience in the field that dust emission is largely restricted to the exposed diatomite sediment. The flux F across this transect therefore represents emission and transport from all exposed diatomite upwind of the site. The region upwind of this transect represents ~8.3% of the entire area of $\sim 10.8 \times 10^9 \text{ m}^2$ of exposed diatomite (defined from identification of diatomite on MODIS surface reflectance data). If we scale our estimate of F accordingly we estimate the dust flux from entire Bodélé diatomite sediment to be 3.5 Tg during the BoDEx 3 day dust event, or $1.18 \pm 0.45 \text{ Tg per day}$. The uncertainty here is estimated from the SE of the regression coefficients and an assumption of a 10% error in calculation of the diatomite density and in each of the diatomite area and transect dimensions. The calculation assumes that dust emission rates over the entire diatomite region are similar to those at the field site. This assumption is untested but plausible, given (1) observations of AOT taken simultaneously on 11 March at the field site and a location some 30 km to the northwest (i.e., along the cross section) are very similar (not shown), (2) wind speeds simulated by the MM5 model indicate that the mean wind speed during 10–12 March averaged over the entire region 16.5–18.5°E, 17.0–17.5°N (encompassing the Bodélé sediment) is within 1% of that for the field location, (3) dust concentration in the dust plume increases from NE–SW across the Bodélé, (assuming that the brightness of the plume in the MODIS imagery is indicative of dust loading) such that peak dust flux occurs on the southwest extremity of the diatomite region (Figure 2c), and (4) estimates of long-term mean AOT from the MISR instrument during the winter months show a peak located near 16°E, 16.5°N (not shown), i.e., near the downwind extremity of the diatomite. Nevertheless, the possibility that surface emission processes may vary within the diatomite region must be recognised,

especially given the predominance of barchan dunes in the north and east of the diatomite. Therefore the assumption of uniform emission is a major but unquantified source of uncertainty in our estimates.

[28] The Bodélé Depression emits dust plumes on approximately 100 days per year [Washington *et al.*, 2006]. We estimate the long-term average emission by applying the technique described above to 6 hourly surface wind data from the NCEP reanalysis data set, using the grid cell centered on the Bodélé. The NCEP wind speeds are corrected for the observed negative bias in this region [Koren and Kaufman, 2004; Washington *et al.*, 2006] by linear regression with our observations over the BoDEx period. The annual mean dust emission over the period 1979–2005 is estimated to be around $182 \pm 65 \text{ Tg yr}^{-1}$. Note that the error values here are based on the same assumptions as in the estimation for the BoDEx period and do not include the errors associated with uncertainty surrounding the linear correction of NCEP wind speeds. Numerical simulations from a range of models estimate the global dust emission to be between 1000–3000 Tg yr^{-1} [Zender *et al.*, 2005]. A speculative inference of this, therefore, is that the diatomite sediments of the Bodélé Depression, an area of only about 10,800 km^2 may be responsible for between 6–18% of global dust emission. We must stress, however, that the uncertainty in our estimate is large, particularly given the short period of the BoDEx study, such that the figures should be considered to be preliminary estimates.

7. Summary and Conclusions

[29] The Bodélé Depression of northern Chad is the world's greatest source region of mineral dust into the atmosphere. Detailed information on processes of dust emission and dust optical properties from such sources is vital to efforts to simulate dust radiative forcing as well as retrieval of dust properties from satellite instruments. Accurate simulation of dust emission processes from the Bodélé region (and other similar locations) is a key requirement of global and regional dust models. To date, observations obtained directly from major dust source regions are lacking. In this paper we present results from the BoDEx 2005 experiment, the first field experiment in the Bodélé Depression region to characterise dust properties and emission processes.

[30] Our limited observations indicate that the aerosol loading in this source region is highly variable from day to day. The large dust plume events during BoDEx 2005 were triggered by strong wind events driven by ridging of the Libyan high-pressure cell, confirming the analysis based on satellite data of Washington and Todd [2005]. Imposed on this synoptically driven regional circulation is a pronounced diurnal cycle in wind speeds such that dust emission occurs in pulses of up to 18 hours in duration. This marked diurnal structure has implications for techniques used to estimate dust emission on the basis of satellite observations from low-Earth orbiting satellites with a fixed local crossing time such as TOMS and MODIS.

[31] From measurements of wind speed, AOT and visual observations during BoDEx 2005 we determine the specific threshold wind speed (15 min average at 2 m height) for

dust emission to be 10.0 ms^{-1} . This value is unusually high in comparison to other dust source regions. Moreover, many global atmospheric models (including those used to generate the NCEP and ERA-40 reanalysis data sets) underestimate surface and LLJ wind speeds over the Bodélé by $\sim 50\%$ [Koren and Kaufman, 2004; Washington *et al.*, 2006]. This may lead dust models to seriously underestimate dust emission from the Bodélé given the highly nonlinear relationship between wind speed and dust flux. There is therefore a clear need for validation of higher-resolution GCMs and/or regional climate models used to drive dust simulations in this region and to appropriate parameterisation of emission processes [Tegen *et al.*, 2006].

[32] SEM analysis of airborne dust material confirms that the dust is predominantly composed of fragments of fossil diatoms. The magnitude of dust emission during large events was beyond the measuring ability of the surface based photometer instruments. However, from our sample of relatively clear and moderate dust event conditions we have determined important aerosol properties from the Bodélé source region. The physical properties indicate that the dominant coarse mode of the particle size distribution of dust from the Bodélé (centered on 1–2 μm) is actually characteristic of other Saharan dust observation despite the unusual characteristics of the Bodélé diatomite sediment. However, there is minor but noticeable presence of particles with radii $< 1 \mu\text{m}$ which is rather unusual for desert dust.

[33] The single-scattering albedo of Bodélé dust is very high with relatively low wavelength dependence. Bearing in mind the rather small sample the results are broadly similar to that previously observed in some other regions in the western Sahara desert. This is particularly interesting because of the specific elemental composition of the Bodélé diatomite. It would therefore be interesting to determine the extent to which the other preferential source regions in the western Sahara [Prospero *et al.*, 2002; Washington *et al.*, 2003] may actually be paleolake beds similar to but smaller than the Bodélé Depression. There is also some evidence that dust from the Ennedi region has lower single-scattering albedo especially in the blue wavelengths, which requires further investigation. The net radiative effect at the surface of high dust loadings (with AOT values in excess of 3.0) causes a large reduction in the surface maximum temperature of $\sim 7^\circ\text{C}$.

[34] On the basis of our observations of dust properties and wind speeds we estimate the daily dust emission during the large 3 day event during BoDEx to be $1.18 \pm 0.45 \text{ Tg d}^{-1}$. Whilst the uncertainty associated with this is high, it represents the first estimate based on direct field observations. With this caveat in mind we may speculate that the Bodélé may be responsible for 6–18% of global dust emissions. Consistency between observations at Bodélé and Ilorin, Nigeria, provides compelling evidence of dust transport from the Bodélé up to distances of at least 1700 km. On the basis of trajectory analysis [Swap *et al.*, 1992; Washington *et al.*, 2006] and satellite estimates [e.g., Kaufman *et al.*, 2005] it is highly likely that dust is transported much farther, as far as South America. Analysis of the geochemistry and mineralogy of dust from Bodélé obtained during BoDEx 2005 will help determine the extent to which this dust is transported to the Amazon and its potential role in ocean and land fertilization.

[35] The observations obtained from BoDEx 2005 are currently being used by the project team and other collaborators to constrain more precisely model simulations of dust emission, transport and climate impact [Teegen *et al.*, 2006]. Finally, we must stress the important caveat that the results presented here are based on a data set of rather limited duration which is unlikely to be fully representative of all seasons and conditions. Further observations are required from this unique and fascinating location to complement the findings here.

[36] **Acknowledgments.** BoDEx 2005 was supported by the Gilchrist Educational Trust with the Gilchrist Fieldwork Award, administered by the Royal Geographical Society (with the Institute of British Geographers). Andrew Wilson of the Centre for Ecology and Hydrology, UK, kindly supplied the Cimel instrument for this project. Thanks are due to the Aeronet team notably Brent Holben, Wayne Newcomb, and Mikhail Sorokin of NASA Aeronet (for calibration and repair of the Cimel), and to Zahra Chaudry for transporting the instrument. We thank Rachel T. Pinker for her effort in establishing and maintaining Aeronet Ilorin site. NERC EPFS and NASA GSFC are acknowledged for providing the Microtops instruments. SEM analysis kindly conducted by S.H. Coetzee at the Electron Microscope Unit, Dept. of Physics, University of Botswana, with help from Frank Eckart. Ilan Koren kindly supplied the MODIS imagery. Finally, we are greatly indebted to Mahamat Aberraham Troumba for logistical support in Chad.

References

- Collins, W. D., P. J. Rasch, B. E. Eaton, B. V. Khattatov, J. F. Lamarque, and C. S. Zender (2001), Simulating aerosols using a chemical transport model with assimilation of satellite aerosol retrievals: Methodology for INDOEX, *J. Geophys. Res.*, *106*, 7313–7336.
- Dubovik, O., and M. D. King (2000), A flexible inversion algorithm for retrieval of aerosol optical properties from Sun and sky radiance measurements, *J. Geophys. Res.*, *105*, 20,673–20,696.
- Dubovik, O., B. N. Holben, T. F. Eck, A. Smirnov, Y. J. Kaufman, M. D. King, D. Tanre, and I. Slutsker (2002a), Variability of absorption and optical properties of key aerosol types observed in worldwide locations, *J. Atmos. Sci.*, *59*, 590–608.
- Dubovik, O., B. N. Holben, T. Lapyonok, A. Sinyuk, M. I. Mishchenko, P. Yang, and I. Slutsker (2002b), Non-spherical aerosol retrieval method employing light scattering by spheroids, *Geophys. Res. Lett.*, *29*(10), 1415, doi:10.1029/2001GL014506.
- Dubovik, O., *et al.* (2006), The application of spheroid models to account for aerosol particle non-sphericity in remote sensing of desert dust, *J. Geophys. Res.*, *111*, D11208, doi:10.1029/2005JD006619.
- Dudhia, J. (1993), A non-hydrostatic version of the Penn State/NCAR Mesoscale model: Validation tests and simulation of an Atlantic cyclone and cold front, *Mon. Weather Rev.*, *121*, 1493–1513.
- Giles, J. (2005), The dustiest place on Earth, *Nature*, *434*, 816–819.
- Gillette, D. A. (1977), Fine particulate emissions due to wind erosion, *Trans. ASAE*, *29*, 890–897.
- Ginoux, P., M. Chin, I. Tegen, J. Prospero, B. Holben, O. Dubovik, and S. J. Lin (2001), Sources and distributions of dust aerosols simulated with the GOCART model, *J. Geophys. Res.*, *106*, 20,255–20,273.
- Goudie, A. S., and N. J. Middleton (1992), The changing frequency of dust storms through time, *Clim. Change*, *20*, 197–225.
- Grell, G. A., J. Dudhia, and D. R. Stauffer (1994), A description of the fifth-generation Penn State-NCAR mesoscale model (MM5), *Tech. Note NCAR/TN-23 398+STR*, 117 pp., Natl. Cent. Atmos. Res., Boulder, Colo.
- Haywood, J. M., P. N. Francis, M. D. Glew, O. Dubovik, and B. N. Holben (2003a), Comparison of aerosol size distributions, radiative properties, and optical depths determined by aircraft observations and Sun photometers during SAFARI-2000, *J. Geophys. Res.*, *108*(D13), 8471, doi:10.1029/2002JD002250.
- Haywood, J. M., *et al.* (2003b), Radiative properties and direct radiative effect of Saharan dust measured by the C-130 aircraft during SHADE: 1. Solar spectrum, *J. Geophys. Res.*, *108*(D18), 8577, doi:10.1029/2002JD002687.
- Haywood, J. M., R. P. Allan, I. Culverwell, T. Slingo, S. Milton, and J. Edwards (2005), Can desert dust explain the outgoing longwave radiation anomaly over the Sahara during July 2003?, *J. Geophys. Res.*, *110*, D05105, doi:10.1029/2004JD005232.
- Herman, J. R., P. K. Bhartia, O. Torres, C. Hsu, C. Sefort, and E. Celarier (1997), Global distribution of UV-absorbing aerosols from Nimbus 7/Toms data, *J. Geophys. Res.*, *102*, 16,911–16,922.
- Highwood, E. J., J. M. Haywood, M. D. Silverstone, S. M. Newman, and J. P. Taylor (2003), Radiative properties and direct effect of Saharan dust measured by the C-130 aircraft during SHADE. 2: Terrestrial spectrum, *J. Geophys. Res.*, *108*(D18), 8578, doi:10.1029/2002JD002552.
- Holben, B. N., *et al.* (1998), AERONET—A federated instrument network and data archive for aerosol characterization, *Remote Sens. Environ.*, *66*, 1–16.
- Hsu, N. C., J. R. Herman, and C. Weaver (2000), Determination of radiative forcing of Saharan dust using combined TOMS and ERBE data, *J. Geophys. Res.*, *105*, 20,649–20,661.
- Kaufman, Y. J., D. Tanre, O. Dubovik, A. Karnieli, and L. A. Remer (2001), Absorption of sunlight by dust as inferred from satellite and ground-based remote sensing, *Geophys. Res. Lett.*, *28*, 1479–1483.
- Kaufman, Y. J., I. Koren, L. A. Remer, D. Tanre, P. Ginoux, and S. Fan (2005), Dust transport and deposition observed from Terra-Moderate resolution Spectroradiometer (MODIS) spacecraft over the Atlantic Ocean, *J. Geophys. Res.*, *110*, D10S12, doi:10.1029/2003JD004436.
- Kinne, S., *et al.* (2003), Monthly averages of aerosol properties: A global comparison among models, satellite data, and AERONET ground data, *J. Geophys. Res.*, *108*(D20), 4634, doi:10.1029/2001JD001253.
- Koren, I., and Y. J. Kaufman (2004), Direct wind measurements of Saharan dust events from Terra and Aqua satellites, *Geophys. Res. Lett.*, *31*, L06122, doi:10.1029/2003GL019338.
- Koren, I., Y. J. Kaufman, R. Washington, M. C. Todd, Y. Rudich, V. J. Martins, and D. Rosenfeld (1998), The Bodélé depression: a single spot in the Sahara that provides most of the mineral dust to the Amazon forest?, *Environ. Res. Lett.*, *1*, doi:10.1088/1748-9326/1/1/014005.
- Miller, R. L., and I. Tegen (1998), Climate response to soil dust aerosols, *J. Clim.*, *11*, 3247–3267.
- Moody, E. G., M. D. King, S. Platnick, C. B. Schaafa, and F. Gao (2005), Spatially complete global spectral surface albedos: Value-added datasets derived from terra MODIS land products, *IEEE Trans. Geosci. Remote Sens.*, *43*, 144–158.
- Myhre, G., A. Grini, J. M. Haywood, F. Stordal, B. Chatenet, D. Tanré, J. K. Sundet, and I. S. A. Isaksen (2003), Modelling the radiative impact of mineral dust during the Saharan Dust Experiment (SHADE) campaign, *J. Geophys. Res.*, *108*(D18), 8579, doi:10.1029/2002JD002566.
- Park, S. U., and H. E. In (2003), Parameterization of dust emission for the simulation of the yellow sand (Asian dust) event observed in March 2002 in Korea, *J. Geophys. Res.*, *108*(D19), 4618, doi:10.1029/2003JD003484.
- Pinker, R. T., G. Pandithurai, B. N. Holben, O. Dubovik, and T. O. Aro (2001), A dust outbreak episode in sub-Sahel West Africa, *J. Geophys. Res.*, *106*, 22,923–22,930.
- Prospero, J. M., and P. J. Lamb (2003), African droughts and dust transport to the Caribbean: Climate change implications, *Science*, *302*(5647), 1024–1027.
- Prospero, J. M., P. Ginoux, O. Torres, S. E. Nicholson, and T. E. Gill (2002), Environmental characterization of global sources of atmospheric soil dust identified with the NIMBUS 7 Total Ozone Mapping Spectrometer (TOMS) absorbing aerosol product, *Rev. Geophys.*, *40*(1), 1002, doi:10.1029/2000RG000095.
- Ramaswamy, V., O. Boucher, J. Haigh, D. Hauglustaine, J. Haywood, G. Myhre, T. Nakajima, G. Y. Shi, and S. Solomon (2001), Radiative forcing of climate change, Chapter 6 in *IPCC Climate Change 2000, The Science of Climate Change*, edited by J. T. Houghton *et al.*, 881 pp., Cambridge Univ. Press, New York.
- Smirnov, A., B. N. Holben, I. Slutsker, E. J. Welton, and P. Formenti (1998), Optical properties of Saharan dust during ACE 2, *J. Geophys. Res.*, *103*, 28,079–28,092.
- Smirnov, A., B. N. Holben, T. F. Eck, O. Dubovik, and I. Slutsker (2000), Cloud screening and quality control algorithms for the AERONET database, *Remote Sens. Environ.*, *73*, 337–349.
- Swap, R., M. Garstang, S. Greco, R. Talbot, and P. Kaallberg (1992), Saharan dust in the Amazon basin, *Tellus, Ser. B*, *44*, 133–149.
- Tanré, D., *et al.* (2003), Measurement and modeling of the Saharan dust radiative impact: Overview of the Saharan Dust Experiment (SHADE), *J. Geophys. Res.*, *108*(D18), 8574, doi:10.1029/2002JD003273.
- Tegen, I., and I. Fung (1994), Modelling mineral dust in the atmosphere: Sources, transport and optical thickness, *J. Geophys. Res.*, *99*, 22,897–22,914.
- Tegen, I., P. Hollrig, M. Chin, I. Fung, D. Jacob, and J. Penner (1997), Contribution of different aerosol species to the global aerosol extinction optical thickness: Estimates from model results, *J. Geophys. Res.*, *102*, 23,895–23,915.
- Tegen, I., S. P. Harrison, K. Kohfeld, I. C. Prentice, M. Coe, and M. Heimann (2002), Impact of vegetation and preferential source areas on global dust aerosol: Results from a model study, *J. Geophys. Res.*, *107*(D21), 4576, doi:10.1029/2001JD000963.

- Tegen, I., B. Heinold, M. C. Todd, J. Helmert, R. Washington, and O. Dubovik (2006), Modeling soil dust aerosol in the Bodélé Depression during BoDEx 2005, *Atmos. Chem. Phys.*, *6*, 4345–4349.
- Torres, O., P. K. Bhartia, J. R. Herman, A. Sinyuk, and B. Holben (2002), A long term record of aerosol optical thickness from TOMS observations and comparison to AERONET measurements, *J. Atmos. Sci.*, *59*, 398–413.
- Washington, R., and M. C. Todd (2005), Atmospheric controls on mineral dust emission from the Bodélé Depression, Chad: Intraseasonal to inter-annual variability and the role of the Low Level Jet, *Geophys. Res. Lett.*, *32*, L17701, doi:10.1029/2005GL023597.
- Washington, R., M. C. Todd, N. Middleton, and A. S. Goudie (2003), Dust-storm source areas determined by the total ozone monitoring spectrometer and surface observations, *Ann. Assoc. Am. Geogr.*, *93*, 297–313.
- Washington, R., M. C. Todd, S. Engelstaedter, S. Mbainayel, and F. Mitchell (2006), Dust and the low-level circulation over the Bodélé Depression, Chad: Observations from BoDEx 2005, *J. Geophys. Res.*, *111*, D03201, doi:10.1029/2005JD006502.
- Weaver, C., P. Ginoux, N. C. Hsu, M. D. Chou, and J. Joiner (2002), Radiative forcing of Saharan dust: GOCART model simulations compared with ERBE data, *J. Atmos. Sci.*, *59*, 736–747.
- Zender, C. S., H. Bian, and D. Newman (2003), Mineral Dust Entrainment and Deposition (DEAD) model: Description and 1990s dust climatology, *J. Geophys. Res.*, *108*(D14), 4416, doi:10.1029/2002JD002775.
- Zender, C. S., R. L. Miller, and I. Tegen (2005), Quantifying mineral dust mass budgets: Terminology, constraints and current estimates, *Eos, Trans. AGU*, *85*, 6–7.
- Zhang, J., and S. A. Christopher (2003), Longwave radiative forcing of Saharan dust aerosols estimated from MODIS, MISR, and CERES observations on Terra, *Geophys. Res. Lett.*, *30*(23), 2188, doi:10.1029/2003GL018479.

O. Dubovik, NASA Goddard Space Flight Center, Greenbelt, MD 20771, USA.

S. Engelstaedter and R. Washington, Climate Research Laboratory, Oxford University Centre for the Environment, University of Oxford, Oxford, OX1 3QY, UK.

G. Lizcano and M. C. Todd, Department of Geography, University College London, Pearson Building, Gower Street, London WC1E 6BT, UK. (mtodd@geog.ucl.ac.uk)

J. V. Martins, University of Maryland Baltimore County, Baltimore, MD 21250, USA.

S. M'Bainayel, Direction des Ressources en Eau et de la Météorologie (DREM), BP 429 N'Djamena, Chad.